Fast Direct Torque Control of an Open-End Induction Motor Drive Using 12-Sided Polygonal Voltage Space Vectors

Chintan Patel, *Student Member, IEEE*, Rajeevan P. P., Anubrata Dey, Rijil Ramchand, *Student Member, IEEE*, K. Gopakumar, *Senior Member, IEEE*, and Marian P. Kazmierkowski, *Fellow, IEEE*

***Abstract*—A torque control scheme, based on a direct torque control (DTC) algorithm using a 12-sided polygonal voltage space vector, is proposed for a variable speed control of an open-end induction motor drive. The conventional DTC scheme uses a stator flux vector for the sector identification and then the switching vector to control stator flux and torque. However, the proposed DTC scheme selects switching vectors based on the sector information of the estimated fundamental stator voltage vector and its relative position with respect to the stator flux vector. The fundamental stator voltage estimation is based on the steady-state model of IM and the synchronous frequency of operation is derived from the computed stator flux using a low-pass filter technique. The proposed DTC scheme utilizes the exact positions of the fundamental stator voltage vector and stator flux vector to select the optimal switching vector for fast control of torque with small variation of stator flux within the hysteresis band. The present DTC scheme allows full load torque control with fast transient response to very low speeds of operation, with reduced switching frequency variation. Extensive experimental results are presented to show the fast torque control for speed of operation from zero to rated.**

***Index Terms*—Adjustable speed drives, direct torque control, harmonics eliminations, induction motor drives.**

I. Introduction

ELECTRICAL vehicle applications require frequent torque control to adjust the speed of a vehicle. This has resulted in the need for a control scheme with high performance, fast transient, and accurate control of torque for an induction motor drive. The two most popular schemes for this are the vector control and the direct torque control (DTC) [1], [2]. The DTC schemes proposed by [3], and [4] (as a direct self-control) have several variations to the original structure, such as to overcome the inherent disadvantages in any hysteresis-based controller with variable switching frequency, high sampling requirement for digital implementation, and high torque ripple [5]–[11] Recently, predictive control strategy [12]–[14], dithering technique [15], sliding mode control [16], fuzzy logic control [17], and support vector machine (SVM) [10], [18]–[20] have found applications in motor drives. Furthermore, the use of these control schemes during a large step change in torque command does not guarantee the fastest torque response.

During large torque demand, it is inevitable that the stator voltage reference exceeds the voltage vector limits enclosed by the hexagonal boundary. Under this condition, the SVM has to be operated in what is termed as dynamic over modulation mode. These methods have managed to minimize the voltage vector error as well as obtain a fast torque response; however, the majority of them do not guarantee the fastest torque response.

In all hysteresis-based DTC, the hexagonal-based voltage vectors are selected for torque control. This paper proposes a DTC scheme for an IM drive using a 12-sided polygonal space vector-based inverter with estimated fundamental stator voltage vector for sector identification. In this paper, the sector information for an inverter output is selected with computed fundamental stator voltage. At low speed, stator resistance drop becomes very dominant and the fundamental stator voltage can be in any of the sectors between 0° and 90° with respect to the stator flux vector. In the proposed scheme, the flux and torque control based on the new sector selection technique (at a very low speed of operation) with an appropriate switching table are also presented. The present DTC scheme has an increased modulation range with reduced hysteresis switching frequency variation and allows the full load torque control with fast transient response to a very low speed below 5 Hz. This scheme can be applied easily to an electrical vehicle application due to fast torque control for full range of speed from zero to rated in both directions of rotation.

II. Principle of Direct Torque Control of an Induction Motor

The electromagnetic torque in the three-phase induction machine can be expressed as follows:

$$T_d = \frac{2}{3}\frac{P}{2}\frac{L_m}{L_s L_r - L_m^2}\vec{\psi}_s \times \vec{\psi}_r \tag{1}$$

Manuscript received March 29, 2011; revised May 16, 2011; accepted June 4, 2011. Date of current version December 16, 2011. Recommended for publication by Associate Editor K. L. Ralph.

C. Patel is with PEMC Group, Division of Electrical Systems and Optics, The University of Nottingham, Nottingham, NG7 2RD, U.K. (e-mail: chintanbhai.patel@nottingham.ac.uk).

Rajeevan P. P., A. Day, and K. Gopakumar are with Center for Electronics Design and Technology, Indian Institute of Science, Bangalore 560012, India (e-mail: prajeev@cedt.iisc.ernet.in; adey@cedt.iisc.ernet.in; kgopa@cedt.iisc.ernet.in).

R. Ramchand is with Department of Electrical Engineering, National Institute of Technology, Calicut, Kerala 673601, India (e-mail: rijil@nitc.ac.in).

M. P. Kazmierkowski is with the Institute of Control and Industrial Electronics, Warsaw University of Technology UI, KOS2ykowa 45, 00-662 Warsaw, Poland and he is member of Polish Academy of Science (e-mail: mpk@isep.pw.edu.pl).

Digital Object Identifier 10.1109/TPEL.2011.2159516

where $\vec{\psi}_s$ and $\vec{\psi}_r$ are the stator and rotor flux vectors (both fixed to the stationary reference frame which is fixed to the A-phase axis of a stator), L_m is the magnetizing inductance, L_s is the stator inductance, L_r is the rotor inductance, and P is the number of poles.

Equation (1) can be modified and expressed as

$$T_d = \frac{2}{3}\frac{P}{2}\frac{L_m}{L_s L_r - L_m^2}\left|\vec{\psi}_s\right|\left|\vec{\psi}_r\right|\sin(\rho_s - \rho_r) \qquad (2)$$

where ρ_s is the stator flux angle and ρ_r is the rotor flux angle, both referred to the horizontal axis of the stationary frame fixed to the stator. It is well known that, by keeping the stator flux magnitude constant, the electromagnetic torque can be rapidly changed and controlled by means of changing the angle $(\rho_s - \rho_r)$ [21].

III. DTC of an Induction Motor Using the Fundamental Stator Voltage for Sector Identification

The DTC scheme for an induction motor drive is presented here with modification in a sector selection process, using the fundamental stator voltage vector for sector identification. The proposed DTC scheme also uses a 12-sided polygonal voltage space vector-based inverter [22] for control. A better torque control can be achieved using 12-sided polygonal space vectors compared to a conventional hexagonal space vector. The conventional DTC scheme, using a hexagonal voltage space vector [3], [4], uses the stator flux vector for sector identification and switching vector located around 90° (i.e., orthogonal) to stator flux vector for controlling stator flux and torque. But the stator flux and fundamental stator voltage vector will not always be orthogonal, especially at low speeds of operation. The fundamental stator voltage for an induction motor can be written as

$$\vec{v}_{s,f} = R_s\vec{i}_{s,f} + j\omega_s\vec{\psi}_s. \qquad (3)$$

From (3), it can be noted that at low speeds of operation the drop due to a stator resistance is larger than the drop due to a stator flux. So, the stator resistance drop cannot be ignored for low frequency of operation (typically below 5 Hz). At low speeds, the angle between the stator flux vector and the fundamental stator voltage vector is less than 90° and this angle decreases as the frequency or operation decreases toward zero. Hence, the orthogonal switching vector selection based on the stator flux vector position is not valid for low frequencies of operation. In this paper, the proposed DTC scheme selects the switching vector based on the present sector of the fundamental stator voltage vector and current states of the flux hysteresis controller and the torque hysteresis controller. This scheme of switching vector selection based on the fundamental stator voltage vector position rather than the stator flux vector position allows torque control down to a very low speed (i.e., below 1 Hz) of operation. The relative positions of the stator flux vector and fundamental stator voltage vector (sector information) are used to select the switching vector for the present DTC scheme. This is defined using the scalar product of two vectors. The value of the scalar product is assigned using variable γ (see Section III-D). The fundamental stator voltage vector is estimated using the standard steady-state model for the machine.

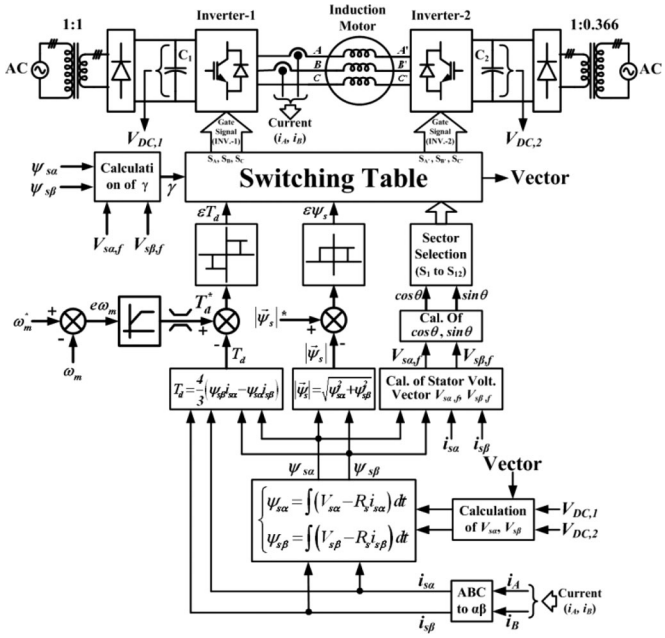

Fig. 1. Control scheme of DTC with the fundamental stator voltage vector for sector identification using 12-sided polygonal space vector-based open-end induction motor drives.

A. Power Circuit and Control Scheme With the Fundamental Stator Voltage Vector-Based DTC

The basic block diagram of the direct torque-controlled induction motor drive using a fundamental stator voltage vector is presented in Fig. 1. The main blocks of the control scheme are torque comparator, flux comparator, optimal switching logic and fundamental stator voltage vector estimator, and stator voltage sector selection. The main difference in the control scheme here is in the calculation of the fundamental stator voltage vector and then in the selection of the sector. The inputs to the sector selection block are $v_{s\alpha,f}$ and $v_{s\beta,f}$ in place of $\psi_{s\alpha}$ and $\psi_{s\beta}$. The values of the stator flux and torque are estimated using a stator voltage and torque equation of an induction motor model, respectively. The values of the stator current and stator voltage vectors are taken from measurements of two-phase currents and dc-link voltages of inverter-1 and inverter-2.

Shaft speed is sensed with an encoder and the reference torque T_d^* is derived from the speed controller output. The flux reference is also given directly as an input signal and the torque and flux references are compared with the estimated values of torque and stator flux magnitudes to find hysteresis controller states. Control signals for the generation of switching signals for both inverters are produced by using a two-level hysteresis control for a stator flux error and a three-level hysteresis control for a torque error. Optimum switching is determined for every control cycle based on the states of flux hysteresis controller, torque hysteresis controller, and present sector information of the fundamental stator voltage vector and relative position of stator flux, using optimal switching table. There are four switching

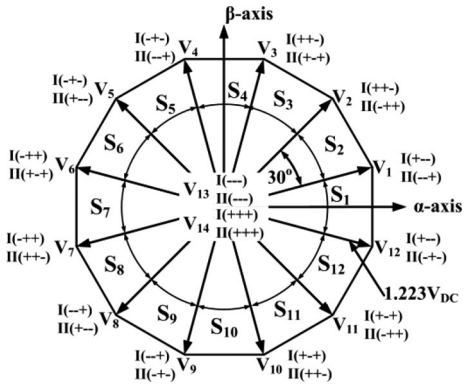

Fig. 2. Resultant 12-sided polygonal space vector positions of the combined inverters and sector identification.

tables based on the relative position of a stator flux with respect to the fundamental stator voltage, for various speeds down to zero. There are six possible conditions for selection of a switching vector based on states of stator flux hysteresis controller and torque hysteresis controller for each sector of fundamental stator voltage position in each switching table and there are 12 sectors for the position of the fundamental stator voltage vector. The switch references (S_A, S_B, S_C) and ($S_{A'}$, $S_{B'}$, $S_{C'}$) for the inverter power module are the outputs of switching logic as shown in Fig. 1. The information of the states of the power switches are used in the calculation of the actual voltage vector for the estimation of stator flux.

The power circuit is realized with a standard two-level inverter power module as shown in Fig. 1. Both inverters are fed from a three-phase rectifier through an isolation transformer to avoid common mode current. The voltage ratio of the two dc-link sources is 1:0.366 to generate the vector location of a 12-sided polygonal voltage space vector [22]. The resultant 14 voltage space vectors with respective switching states of inverter-1 and inverter-2 are shown in Fig. 2. Out of 14 voltage space vectors, $\vec{V}_1$, $\vec{V}_2$, ... ,$\vec{V}_{12}$ are the active voltage vectors, and $\vec{V}_{13}$ and $\vec{V}_{14}$ are the zero voltage vectors [22].

B. Estimation of Stator Flux $\vec{\psi}_s$, Electromagnetic Torque T_d, and Hysteresis Controller for Stator Flux and Torque

The torque and stator flux are estimated using the sensed dc-link voltage and stator currents. The equation for stator flux estimation is given as

$$\vec{\psi}_s = \int \left(\vec{V}_K - R_s \vec{i}_s\right) dt \tag{4}$$

where $\vec{\psi}_s = (\psi_{s\alpha} + j\psi_{s\beta})$ is the estimated stator flux vector, $\vec{V}_K = (V_{K\alpha} + jV_{K\beta})$ is the instantaneous voltage space vector from an inverter, and $\vec{i}_s = (i_{s\alpha} + ji_{s\beta})$ is the stator current.

For flux estimation, the ideal method is integration, but the disadvantages of open integration have been addressed many times in the literature [23]–[26]. The structure for the stator flux estimation scheme is given in Fig. 3. In the block diagram of Fig. 3, if $\psi^*_{s\alpha}$ is made zero, the estimation scheme behaves like an low pass filter (LPF) and introduces phase and magnitude

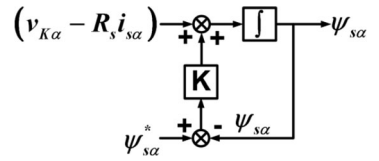

Fig. 3. Block diagram for realization of stator flux estimation.

error. However, the estimation scheme behaves like a high-pass filter for any dc drift occurring at the integrator output.

The components' α- and β-axis stator flux positions are derived as

$$\cos(\omega_s t) = \cos\rho_s = \frac{\psi_{s\alpha}}{\sqrt{\psi^2_{s\alpha} + \psi^2_{s\beta}}} \tag{5}$$

$$\sin(\omega_s t) = \sin\rho_s = \frac{\psi_{s\beta}}{\sqrt{\psi^2_{s\alpha} + \psi^2_{s\beta}}}. \tag{6}$$

The values of $\psi^*_{s\alpha}$ and $\psi^*_{s\beta}$ have to be calculated for the decaying effect. The values of $\psi^*_{s\alpha}$ and $\psi^*_{s\beta}$ can be expressed as $\psi^*_{s\alpha} = |\psi^*_s|\cos\rho_s$ and $\psi^*_{s\beta} = |\psi^*_s|\sin\rho_s$.

The estimation of stator flux as in (4) uses the induction motor stator resistance R_s. The variation of these parameters is needed to be considered for accurate control of a drive. For stator resistance adaptation, one of the well-proven stator parameter adaptation schemes from the literature can be easily implemented in the present scheme, with suitable modifications to fit into the present scheme [23], [25], [27], [28].

The torque is estimated as

$$T_d = \frac{2}{3}\frac{P}{2}\left(\psi_{s\alpha} i_{s\beta} - \psi_{s\beta} i_{s\alpha}\right). \tag{7}$$

The reference value of the stator flux magnitude $|\vec{\psi}_s|*$ is compared with that of the estimated flux magnitude, and the error $\varepsilon\psi_s$ is used to determine the next states of the flux hysteresis controller as

$$\varepsilon\psi_s = \begin{cases} 0 & \text{for } \left|\vec{\psi}_s\right| \le \left|\vec{\psi}_s\right|^* - |\Delta\psi_s| \\ 1 & \text{for } \left|\vec{\psi}_s\right| \ge \left|\vec{\psi}_s\right|^* + |\Delta\psi_s|. \end{cases} \tag{8}$$

For speed control mode of operation, the rotor reference speed ω^*_m is compared with the feedback speed ω_m and this error is converted into the reference torque T^*_d by a speed PI controller as shown in Fig. 1. The mechanical speed is derived using an encoder.

The reference torque T^*_d is compared with the estimated torque T_d and the torque error obtained is fed to a three-level hysteresis comparator. The torque error εT_d determines the next states of the torque hysteresis controller as follows.

For counter clockwise rotation

$$\varepsilon T_d = \begin{cases} 1 & \text{for } T_d \le T^*_d - \Delta T_d \\ 0 & \text{for } T_d \ge T^*_d + \Delta T_d. \end{cases} \tag{9}$$

For clockwise rotation

$$\varepsilon T_d = \begin{cases} 0 & \text{for } T_d \le T^*_d - \Delta T_d \\ -1 & \text{for } T_d \ge T^*_d + \Delta T_d. \end{cases} \tag{10}$$

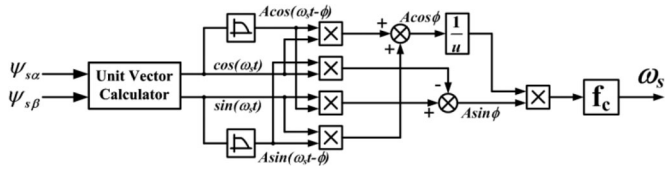

Fig. 4. Estimation of synchronous frequency ω_s using a low-pass filter with cutoff frequency f_c.

C. Estimation of the Fundamental Stator Voltage Vector $\vec{v}_{s,f}$ and the Identification of a Sector

For the steady-state condition, the stator voltage equation can be written as

$$\vec{v}_s = R_s\vec{i}_s + j\omega_s\vec{\psi}_s. \tag{11}$$

Here, the stator flux vector can be estimated and the stator current vector can be sensed directly using a current sensor.

It is possible to estimate synchronous frequency ω_s using the estimated stator flux vector [29]. The block diagram of synchronous frequency ω_s estimation using the estimated stator flux $\vec{\psi}_s$ is shown in Fig. 4.

The cos($\omega_s t$) and sin($\omega_s t$) signals are passed through the filter [28]. The transfer function of the low-pass filter is

$$G(s) = \frac{1}{sT_c + 1} \quad \text{where} \quad T_c = \text{filter time constant}. \tag{12}$$

Equation (12) can be written in terms of frequency ω and complex form as

$$G(s) = \frac{1}{1 + j\omega T_c} = |G(s)|\angle\phi = X + jY \tag{13}$$

where $j\omega = s =$ complex frequency, $|G(s)| = 1/\sqrt{1+\omega^2T_c^2}$, $\phi = -\tan^{-1}\omega T_c$, $X = 1/1+\omega^2T_c^2$, and $Y = -\omega T_c/1+\omega^2T_c^2$.

The output signals and input signals of the low-pass filter are used to calculate cosϕ and sinϕ (see Fig. 4)

$$[\cos(\omega_s t)\, A\cos(\omega_s t - \phi) + \sin(\omega_s t)\, A\sin(\omega_s t - \phi)] = A\cos\phi \tag{14}$$

$$[\sin(\omega_s t)\, A\cos(\omega_s t - \phi) - \cos(\omega_s t)\, A\sin(\omega_s t - \phi)] = A\sin\phi. \tag{15}$$

Now dividing (14) by (15) yields [28]

$$\frac{A\,sin\phi}{A\,\cos\phi} = \omega_s T_c \quad \text{and} \quad \omega_s = \frac{1}{T_C}\frac{A\,\sin\phi}{A\,\cos\phi}.$$

The value of the filter time constant T_c in the proposed DTC scheme is taken as 15.92 ms.

Finally, the fundamental stator voltage vector $\vec{v}_{s,f}$ is estimated using (11) as

$$\vec{v}_{s,f} = v_{s\alpha,f} + jv_{s\beta,f} = R_s\left(i_{s\alpha} + ji_{s\beta}\right) + j\omega_s\left(\psi_{s\alpha} + j\psi_{s\beta}\right) \tag{16}$$

$$\vec{v}_{s,f} = v_{s\alpha,f} + jv_{s\beta,f} = \left(R_s i_{s\alpha} - \omega_s\psi_{s\beta}\right) + j\left(R_s i_{s\beta} + \omega_s\psi_{s\alpha}\right). \tag{17}$$

The 12 active voltage space vectors divide the whole cycle equally into 12 sectors (see Fig. 2).The sector information of the fundamental stator voltage vector $\vec{v}_{s,f}$ is determined using the unit vector of the estimated fundamental stator voltage vector as

$$\cos\theta_s = \frac{v_{s\alpha,f}}{\sqrt{v_{s\alpha,f}^2 + v_{s\beta,f}^2}}, \quad \sin\theta_s = \frac{v_{s\beta,f}}{\sqrt{v_{s\alpha,f}^2 + v_{s\beta,f}^2}} \tag{18}$$

where θ_s is the angle of the fundamental stator voltage vector with respect to the α-axis (see Fig. 2). The values of unit vector components will lie between particular values that define a sector as given in Fig. 2.

D. Switching Strategy for the DTC Scheme and an Optimum Switching Table

When an induction motor is fed from a voltage source inverter, where its output voltage space vector is defined as $\vec{V}_K$, the stator voltage equation with a stator resistance drop neglected can be rewritten as

$$\vec{V}_K = \frac{d\vec{\psi}_s}{dt}. \tag{19}$$

Here, *K* can have a value either of 1,2,. . .,14 (see Fig. 2).

For the output voltage space vector of duration Δt, the change in the stator flux vector will be given as

$$\Delta\vec{\psi}_s = \vec{V}_K\,\Delta t. \tag{20}$$

But the change in magnitude is proportional to the voltage space vector and its time duration.

For different inverter active vectors, the stator flux vector moves by a small amount in the direction of the inverter voltage space vector as shown in Fig. 5. These result in the change of slip speed which in turn changes the torque as well as changes the length of the stator flux vector. For the present condition shown in Fig. 5, the advanced active space vector (i.e., one of voltage space vectors from $\vec{V}_1$ to $\vec{V}_6$) from the present position of the stator flux increases the angle ($\rho_s - \rho_r$) as in (2). Hence, the torque increases due to an increase in slip speed. However, the trailing active vector (i.e., one of voltage space vectors from $\vec{V}_7$ to $\vec{V}_{12}$) decreases the angle ($\rho_s - \rho_r$) and the torque decreases due to a decrease in slip speed. And the active vector at an angle of more than 90° (i.e., one of voltage space vectors from $\vec{V}_4$ to $\vec{V}_9$) with respect to the present position of the stator flux vector will result in decrement of stator flux vector length regardless of the position of the fundamental stator voltage vector. Hence, the nearest active vectors at an angle of more than 90° with respect to the present position of a stator flux vector are always needed for decrement in magnitude of a stator flux vector. But the position of the fundamental stator voltage vector will not be around orthogonal for all operating conditions as can be concluded from (11). The position of the fundamental stator voltage vector will be less than 90° for low speeds of operation.

Hence, the present DTC scheme selects a switching vector according to the present sector information of the fundamental stator voltage vector for torque control. But the switching vectors' positions at an angle of more than 90° with respect to the

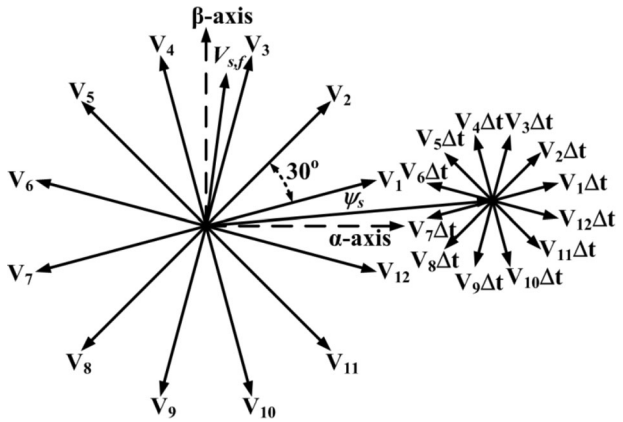

Fig. 5. Effect of the voltage space vector on stator flux for the relative position of the fundamental stator voltage vector and stator flux vector in segment-1 [for $90^\circ \le \chi < 75^\circ$ $(0 \le \gamma < 0.2588)$].

stator flux vector are always selected for flux control, for all speeds of operation.

The relative position of the fundamental stator voltage vector and stator flux vector is calculated using the scalar product (i.e., DOT product) of unit vectors of the fundamental stator voltage vector and stator flux vector. The unit vector of the stator flux is calculated using (5) and (6). The unit vector of the fundamental stator voltage vector is calculated using (18). The scalar product of two unit vector is defined as

$$\hat{\psi}_s \cdot \hat{v}_{s,f} = (\cos\rho_s + j\sin\rho_s)\cdot(\cos\theta_s + j\sin\theta_s)$$
$$\left|\hat{\psi}_s\right| |\hat{v}_{s,f}| \cos(\chi) = (\cos\rho_s + j\sin\rho_s)\cdot(\cos\theta_s + j\sin\theta_s) \quad (21)$$

where $\hat{\psi}_s$ $(=\cos\rho_s + j\sin\rho_s)$ is the unit vector of the stator flux $\vec{\psi}_s$, $\hat{v}_{s,f}$ $(=\cos\theta_s + j\sin\theta_s)$ is the unit vector of the fundamental stator voltage $\vec{v}_{s,f}$, and χ is the angle between $\hat{\psi}_s$ and $\hat{v}_{s,f}$.

Hence, (21) can be written with a unit vector as

$$\hat{\psi}_s \cdot \hat{v}_{s,f} = \cos(\chi) = \cos\rho_s\cos\theta_s + \sin\rho_s\sin\theta_s. \quad (22)$$

Now, the relative position of the voltage vector and stator flux vector can be defined with variable γ as shown in

$$\gamma = \cos(\chi) = \cos\rho_s\cos\theta_s + \sin\rho_s\sin\theta_s. \quad (23)$$

The maximum possible angle χ can be of 90° when the stator resistance drop is negligible or zero (high speeds of operation) compared to the voltage drop due to the stator flux (11). Hence, the value of γ for the maximum and minimum angles is 0 and 1, respectively. This range of the maximum and minimum angles between the fundamental stator voltage vector and the stator flux vector is divided into four segments as given in Table I. And the switching strategy is decided for each segment so that fast control of torque is possible and stator flux could be kept within the hysteresis band.

Fig. 5 shows one of the possible conditions of angle χ for counterclockwise rotation (i.e., forward direction) when the stator flux vector lies just above the α-axis. The position of the

TABLE I
RANGE OF ANGLE χ FOR SEGMENTS DEFINING THE RELATIVE POSITION OF THE STATOR FLUX VECTOR

Segment No.	Range of angle χ	Range of variable γ
Segment - 1	$90^\circ \le \chi < 75^\circ$	$0 \ge \gamma > 0.2588$
Segment - 2	$75^\circ \le \chi < 45^\circ$	$0.2588 \ge \gamma > 0.7071$
Segment - 3	$45^\circ \le \chi < 15^\circ$	$0.7071 \ge \gamma > 0.9659$
Segment - 4	$15^\circ \le \chi \le 0^\circ$	$0.9659 \ge \gamma > 1.0$

fundamental stator voltage vector will change for different segments with the fixed position of the stator flux vector. For the stator flux vector fixed just above the α-axis (see Fig. 5), the fundamental stator voltage vector will be positioned in sector S_4 for segment-1, sector S_3 for segment-2, sector S_2 for segment-3, and sector S_1 for segment-4. The switching strategy of all four segments is decided such that it produces fast torque control and minimum effect in the stator flux. The switching vectors which form sector should be selected to control torque and stator flux as far as possible for the present sector information of the fundamental stator voltage vector.

For the position of Segment-1, the fundamental stator voltage vector positioned approximately orthogonal to the stator flux vector due to a small stator resistance drop as shown in Fig. 5. For the present condition, the most appropriate switching vectors are vector $\vec{V}_3$ and vector $\vec{V}_4$. These two vectors form sector S_4 as shown in Fig. 5. In general, it can be concluded for a segment-1 type of condition that the switching voltage vector which forms the sector needs to be selected to control both torque and stator flux.

For the position of Segment-2, the fundamental stator voltage vector is positioned in sector S_3 for the stator flux vector fixed just above the α-axis (see Fig. 5), which is not orthogonal to the stator flux vector. The present condition is due to comparable stator resistance drop. For the present condition, vectors $\vec{V}_3$ and $\vec{V}_2$ are not the most appropriate switching vectors because both vectors will produce the torque but they will also increase the length of the stator flux vector. Hence, one of vectors $\vec{V}_3$ and $\vec{V}_2$ can be selected for torque control but some other switching vectors need to be selected to control torque as well as decrease the length of the stator flux vector. So, a vector at an angle of more than 90° is selected to control torque and decrease the length of the stator flux vector. Thus, the switching vectors selected are vectors $\vec{V}_2$ and $\vec{V}_4$ for torque and stator flux control, respectively.

For the position of Segment-3, the fundamental stator voltage vector is positioned in sector S_2 which is also not orthogonal to the stator flux vector fixed just above the α-axis (see Fig. 5). The present condition is due to a large effect of stator resistance drop compared to voltage drop due to the stator flux. For the present case, the switching vectors selected are vector $\vec{V}_2$ and vector $\vec{V}_4$ for torque and stator flux control, respectively, same as the switching strategy explained for segment-2.

For the position of Segment-4, the fundamental stator voltage vector is positioned in sector S_1 where the stator flux vector is fixed just above the α-axis (see Fig. 5). The present condition is possible because the effect of stator flux voltage drop is negligible or zero. The fundamental stator voltage vector is

TABLE II
OPTIMAL SWITCHING TABLE FOR THE DTC SCHEME USING FUNDAMENTAL STATOR VOLTAGE

Sector No.	$0.2588 > \gamma \geq 0$						$0.7071 > \gamma \geq 0.2588$					
	$\varepsilon\psi_s = 0$			$\varepsilon\psi_s = 1$			$\varepsilon\psi_s = 0$			$\varepsilon\psi_s = 1$		
	εT_d =-1	εT_d =0	εT_d =1	εT_d =-1	εT_d =0	εT_d =1	εT_d =-1	εT_d =0	εT_d =1	εT_d =-1	εT_d =0	εT_d =1
S_1	V_1	V_{13}/V_{14}	V_{12}	V_{12}	V_{13}/V_{14}	V_1	V_1	V_{13}/V_{14}	V_{12}	V_{11}	V_{13}/V_{14}	V_2
S_2	V_2	V_{13}/V_{14}	V_1	V_1	V_{13}/V_{14}	V_2	V_2	V_{13}/V_{14}	V_1	V_{12}	V_{13}/V_{14}	V_3
S_3	V_3	V_{13}/V_{14}	V_2	V_2	V_{13}/V_{14}	V_3	V_3	V_{13}/V_{14}	V_2	V_1	V_{13}/V_{14}	V_4
S_4	V_4	V_{13}/V_{14}	V_3	V_3	V_{13}/V_{14}	V_4	V_4	V_{13}/V_{14}	V_3	V_2	V_{13}/V_{14}	V_5
S_5	V_5	V_{13}/V_{14}	V_4	V_4	V_{13}/V_{14}	V_5	V_5	V_{13}/V_{14}	V_4	V_3	V_{13}/V_{14}	V_6
S_6	V_6	V_{13}/V_{14}	V_5	V_5	V_{13}/V_{14}	V_6	V_6	V_{13}/V_{14}	V_5	V_4	V_{13}/V_{14}	V_7
S_7	V_7	V_{13}/V_{14}	V_6	V_6	V_{13}/V_{14}	V_7	V_7	V_{13}/V_{14}	V_6	V_5	V_{13}/V_{14}	V_8
S_8	V_8	V_{13}/V_{14}	V_7	V_7	V_{13}/V_{14}	V_8	V_8	V_{13}/V_{14}	V_7	V_6	V_{13}/V_{14}	V_9
S_9	V_9	V_{13}/V_{14}	V_8	V_8	V_{13}/V_{14}	V_9	V_9	V_{13}/V_{14}	V_8	V_7	V_{13}/V_{14}	V_{10}
S_{10}	V_{10}	V_{13}/V_{14}	V_9	V_9	V_{13}/V_{14}	V_{10}	V_{10}	V_{13}/V_{14}	V_9	V_8	V_{13}/V_{14}	V_{11}
S_{11}	V_{11}	V_{13}/V_{14}	V_{10}	V_{10}	V_{13}/V_{14}	V_{11}	V_{11}	V_{13}/V_{14}	V_{10}	V_9	V_{13}/V_{14}	V_{12}
S_{12}	V_{12}	V_{13}/V_{14}	V_{11}	V_{11}	V_{13}/V_{14}	V_{12}	V_{12}	V_{13}/V_{14}	V_{11}	V_{10}	V_{13}/V_{14}	V_1
Sector No.	$0.9659 > \gamma \geq 0.7071$						$1.0 \geq \gamma \geq 0.9659$					
	$\varepsilon\psi_s = 0$			$\varepsilon\psi_s = 1$			$\varepsilon\psi_s = 0$			$\varepsilon\psi_s = 1$		
	εT_d =-1	εT_d =0	εT_d =1	εT_d =-1	εT_d =0	εT_d =1	εT_d =-1	εT_d =0	εT_d =1	εT_d =-1	εT_d =0	εT_d =1
S_1	V_1	V_{13}/V_{14}	V_{12}	V_{10}	V_{13}/V_{14}	V_3	V_{12}	V_1/V_{12}	V_1	V_9	V_{13}/V_{14}	V_4
S_2	V_2	V_{13}/V_{14}	V_1	V_{11}	V_{13}/V_{14}	V_4	V_1	V_2/V_1	V_2	V_{10}	V_{13}/V_{14}	V_5
S_3	V_3	V_{13}/V_{14}	V_2	V_{12}	V_{13}/V_{14}	V_5	V_2	V_3/V_2	V_3	V_{11}	V_{13}/V_{14}	V_6
S_4	V_4	V_{13}/V_{14}	V_3	V_1	V_{13}/V_{14}	V_6	V_3	V_4/V_3	V_4	V_{12}	V_{13}/V_{14}	V_7
S_5	V_5	V_{13}/V_{14}	V_4	V_2	V_{13}/V_{14}	V_7	V_4	V_5/V_4	V_5	V_1	V_{13}/V_{14}	V_8
S_6	V_6	V_{13}/V_{14}	V_5	V_3	V_{13}/V_{14}	V_8	V_5	V_6/V_5	V_6	V_2	V_{13}/V_{14}	V_9
S_7	V_7	V_{13}/V_{14}	V_6	V_4	V_{13}/V_{14}	V_9	V_6	V_7/V_6	V_7	V_3	V_{13}/V_{14}	V_{10}
S_8	V_8	V_{13}/V_{14}	V_7	V_5	V_{13}/V_{14}	V_{10}	V_7	V_8/V_7	V_8	V_4	V_{13}/V_{14}	V_{11}
S_9	V_9	V_{13}/V_{14}	V_8	V_6	V_{13}/V_{14}	V_{11}	V_8	V_9/V_8	V_9	V_5	V_{13}/V_{14}	V_{12}
S_{10}	V_{10}	V_{13}/V_{14}	V_9	V_7	V_{13}/V_{14}	V_{12}	V_9	V_{10}/V_9	V_{10}	V_6	V_{13}/V_{14}	V_1
S_{11}	V_{11}	V_{13}/V_{14}	V_{10}	V_8	V_{13}/V_{14}	V_1	V_{10}	V_{11}/V_{10}	V_{11}	V_7	V_{13}/V_{14}	V_2
S_{12}	V_{12}	V_{13}/V_{14}	V_{11}	V_9	V_{13}/V_{14}	V_2	V_{11}	V_{12}/V_{11}	V_{12}	V_8	V_{13}/V_{14}	V_3

represented only due to stator resistance drop. For the present case, the switching vectors selected are vector $\vec{V}_1$ and vector $\vec{V}_4$ for torque and stator flux control, respectively, same as the switching strategy explained for segment-2 and segment-3.

The optimal switching voltage vector selection most suitable for current states of the flux hysteresis controller and torque hysteresis controller in all sectors is given in Table II. The switching table is formed in such a way that the adjacent switching happens for a particular sector as much as possible. For example, for the stator voltage vector in sector S_1 (i.e., $-15^\circ \leq \theta_s \leq 15^\circ$), the value of γ is between 0.2588 and 0; vectors $\vec{V}_1$ for clockwise rotation or vector $\vec{V}_{12}$ for counterclockwise rotation is selected for an increase in flux magnitude, enabling quick response. Also, vector $\vec{V}_{12}$ for clockwise rotation or vector $\vec{V}_1$ for counterclockwise rotation is applied for a decrease in flux magnitude. For the same sector (S_1), the value of γ is between 0.2588 and 0; vector $\vec{V}_{12}$ or vector $\vec{V}_1$ for either direction of rotation is applied to increase torque. Two zero vectors can be applied to an induction motor in the event of torque reduction.

The zero vector $\vec{V}_{13}$ or vector $\vec{V}_{14}$ is applied for torque reduction for both directions of rotation. One of the zero vectors is selected based on the previous active vector, so there will be the minimum number of switching in pole voltage. Thus, a suitable voltage vector is selected according to the flux and torque requirements with minimum number of switching in pole voltage to give fast torque control.

IV. EXPERIMENTAL RESULTS

The proposed DTC scheme using the fundamental stator voltage based on a 12-sided polygonal space vector is experimentally verified using a 5 HP three-phase open-end winding induction motor drive. The parameters of the motor used for the experimental verification are given in the Appendix. The block diagram in Fig. 1 is used for experimental validation. The control algorithm is implemented using a TM320F2812 DSP processor. The parameters of the hysteresis controller are selected such that the maximum switching frequency is not more than 4 kHz in a linear region of pulsewidth modulation (PWM) operation. The drive has been tested under various working conditions. Figs. 6–10 show the operation of the DTC drive for 1, 30, and 40 Hz frequencies of operation under different operating conditions. The mechanical speed is derived using an encoder.

Figs. 6(a), 8(a), and 10(a) show the experimental result of transient of a DTC drive using the fundamental stator voltage vector during the start-up condition for 1, 30, and 40 Hz operation, respectively. It is seen that after successfully building the flux to the rated value, the drive starts smoothly and reaches the steady-state condition. The drive starts operating into torque control mode instantaneously. It is seen that the torque increases fast and reaches to its reference value. The DTC scheme using the fundamental stator voltage vector allows the successful operation of drive at 1 Hz. It is seen that torque control is possible at low speed (i.e., below 5 Hz) of operation.

Figs. 6(b), 8(b), and 10(b) show the experimental result of a DTC drive using the fundamental stator voltage vector at steady state for 1, 30, and 40 Hz operation, respectively. The torque control is also highly effective as the steady-state speed ripple is within the hysteresis band. The phase voltage waveform with PWM control, from 12-sided voltage space vectors, is shown in Fig. 6(b). The phase voltage waveform has changed because

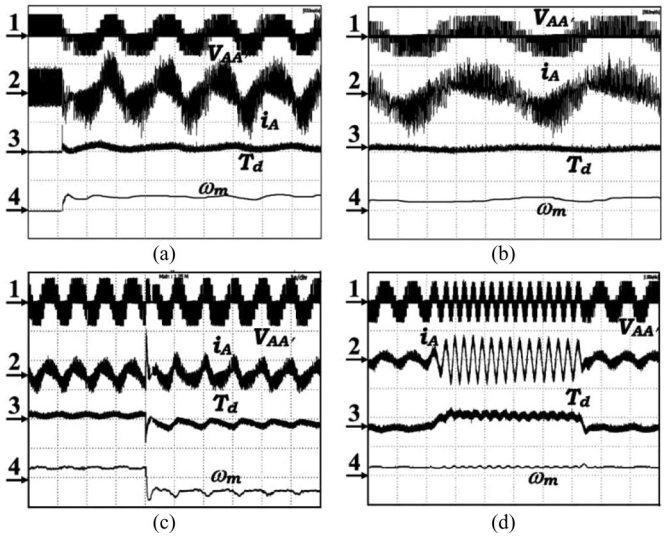

Fig. 6. Experimental result of the DTC drive using fundamental stator voltage for 1 Hz operation. (a) Start-up, (b) steady state, (c) speed reversal, (d) loading: (1) phase voltage $V_{AA'}$, (2) motor phase current i_A, (3) estimated torque T_d, (4) speed of motor ω_m (x-axis: (a) 500 ms/div, (b) 200 ms/div, (c) 1 s/div, (d) 1 s/div; y-axis: (1a), (1b), (1d) 250 V/div, (1c) 200 V/div, (2a), (2b) 1 A/div, (2c) 2 A/div, (2d) 4 A/div, (3) 22.1 N·m/div, (4) 75 (r/min)/div).

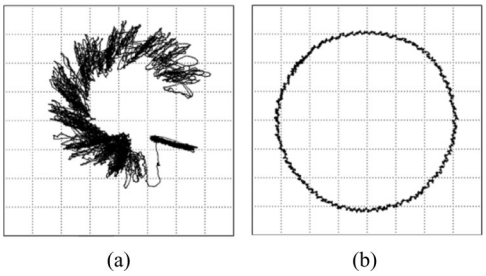

Fig. 7. (a) *XY*-plot of a stator current space phasor at start of drive for 1 Hz operation (x-axis: 1.2 A/div, y-axis: 1.2 A/div). (b) *XY*-plot of estimated stator flux space vector under the steady-state condition for 1 Hz operation (x-axis: 0.5 Wb/div, y-axis: 0.5 Wb/div).

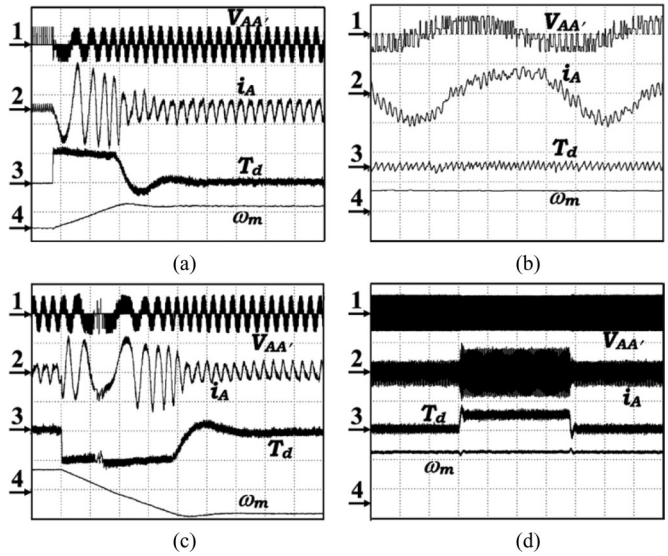

Fig. 8. Experimental result of the DTC drive using fundamental stator voltage for 30 Hz operation. (a) Start-up, (b) steady state, (c) speed reversal, (d) loading: (1) phase voltage $V_{AA'}$, (2) motor phase current i_A, (3) estimated torque T_d, (4) speed of motor ω_m (x-axis: (a) 100 ms/div, (b) 5 ms/div, (c) 100 ms/div, (d) 1 s/div; y-axis: (1) 500 V/div, (2a), (2d) 5 A/div, (2b) 2 A/div, (2c) 6 A/div, (3) 22.1 N·m/div, (4a), (4b), (4c) 1200 (r/min)/div, (4d) 480 (r/min)/div).

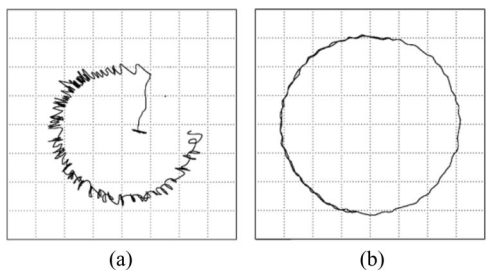

Fig. 9. (a) *XY*-plot of the current space phasor at start of drive for 30 Hz operation (x-axis: 4 A/div, y-axis: 4 A/div). (b) *XY*-plot of the estimated stator flux space vector under the steady-state condition for 30 Hz operation (x-axis: 0.5 Wb/div, y-axis: 0.5 Wb/div).

the angle between the fundamental stator voltage vector and the stator flux vector is less than 90°. Hence, the switching vectors are selected based on the value of variable γ. But the phase current waveform still looks sinusoidal which confirms the sinusoidal flux.

Figs. 6(c) and 8(c) show the experimental result of transient of a DTC drive using the fundamental stator voltage vector during speed reversal from the positive direction to the negative direction of rotation for 1 and 30 Hz operation, respectively. It is seen that the smooth speed reversal is possible with tight control of torque. The proposed DTC scheme adjusts the lookup table based on the relative positions of the fundamental stator voltage vector and stator flux vector using variable γ as given in Table I. It is observed that transition from one segment to other segment occurs smoothly without losing control. It can be seen that the developed torque is controlled at reference torque successfully even at zero speed.

Figs. 6(d), 8(d), and 10(c) show the experimental result of the DTC drive using the fundamental stator voltage vector during the loading condition for 1, 30, and 40 Hz operation, respectively. The DTC drive works perfectly during the loading condition also. It can be seen in the results that torque is controlled around the reference torque successfully, for whole range of speed of operation. Figs. 7(a), 9(a), and 11(a) show the *XY*-plot of the stator current during the starting condition. The stator current is very small during flux building mode and it increases instantaneously to a high value for supplying the reference torque, very quickly. This fast change in the stator current represents the fast torque control.

Figs. 7(b), 9(b), and 11(b) show the *XY*-plot of the estimated stator flux under the steady-state condition. The trajectory is circular for all speeds of operation. The circular trajectory of the stator flux also confirms the successful operation of the proposed DTC scheme to control the stator flux as well.

Fig. 12 shows the experimental results of the DTC drive from 10 Hz operation to zero speed and then accelerate to the set speed of 10 Hz, with small load torque applied. From Fig. 12(a), it is seen that the induction motor

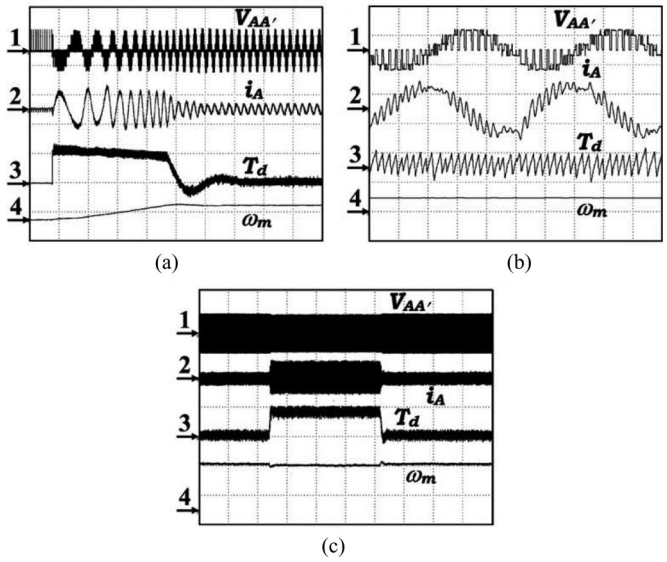

Fig. 10. Experimental result of the DTC drive using fundamental stator voltage for 40 Hz operation. (a) Start-up, (b) steady state, (c) loading: (1) phase voltage $V_{AA'}$, (2) motor phase current i_A, (3) estimated torque T_d, (4) speed of motor ω_m (*x*-axis: (a) 100 ms/div, (b) 5 ms/div, (c) 1 s/div; *y*-axis: (1) 500 V/div, (2a), (2c) 10 A/div, (2b) 2 A/div, (3a), (3c) 22.1 N·m/div, (3b) 11.05 N·m/div, (4a), (4b) 2400 (r/min)/div, (4c) 720 (r/min)/div).

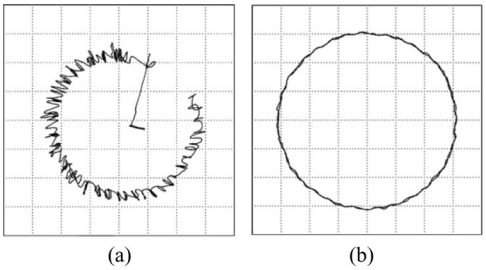

Fig. 11. (a) *XY*-plot of the current space phasor at start of drive for 40 Hz operation (*x*-axis: 4 A/div, *y*-axis: 4 A/div). (b) *XY*-plot of the estimated stator flux space vector under the steady-state condition for 40 Hz operation (*x*-axis: 0.5 Wb/div, *y*-axis: 0.5 Wb/div).

drive comes to a standstill from the speed of 10 Hz (i.e., 300 r/min) successfully with small load. It is seen that the speed is zero at the bottom waveform of Fig. 12(a) and the DTC drive still controls the torque to its reference value without any loss of control. From Fig. 12(b), it is seen that the induction motor drive starts running from standstill to its set speed successfully. It is seen that the speed increases steadily from zero to its set speed of 10 Hz (i.e., 300 r/min). Fig. 13 shows the variation of the reference torque, and the estimated torque for 20 Hz and 40 Hz operation for the starting condition. It also shows that the estimated torque starts following the reference very quickly and the response time of the estimated torque is very fast.

V. Comparison Between Proposed DTC Based on a 12-Sided Polygonal Space Vector and DTC Based on a Hexagonal Space Vector

The comparison of two schemes is done for the torque response and switching frequency variation in a sector. The comparison is done using the simulation analysis for both schemes of DTC. The induction motor specifications are given in the Appendix.

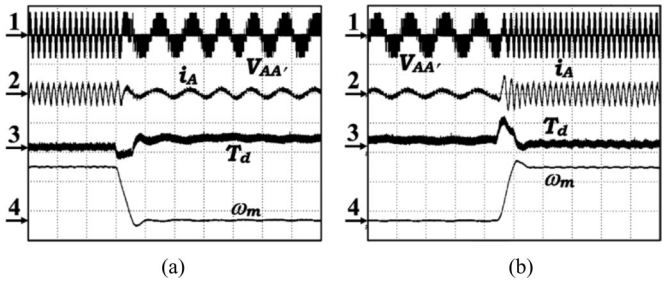

Fig. 12. Experimental result of the DTC drive using fundamental stator voltage for zero speed operation. (a) From 10 Hz to zero speed, (b) from zero speed to 10 Hz: (1) phase voltage $V_{AA'}$, (2) motor phase current i_A, (3) estimated torque T_d, (4) speed of motor ω_m (*x*-axis: (a) 500 ms/div, (b) 500 ms/div; *y*-axis: (1) 200 V/div, (2) 5 A/div, (3) 11.05 N·m/div, (4) 150 (r/min)/div).

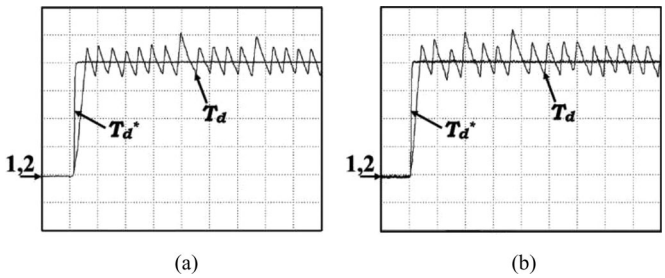

Fig. 13. Result of torque response for the DTC drive using fundamental stator voltage during the start-up condition. (a) 20 Hz operation, (b) 40 Hz operation: (1) reference torque T_d^*, (2) estimated torque T_d (*x*-axis: 2 ms/div, *y*-axis: (1) 5.52 N·m/div, (2) 5.52 N·m/div).

A. Comparison of Torque Responses

The torque response for the proposed DTC based on a 12-sided space vector and the conventional DTC based on a hexagonal space vector is done using simulation. For the comparison study, the torque command is given at a time when the stator flux vector is positioned along the α-axis (i.e., the stator flux vector is in sector-1 in both the cases). The torque response of both schemes during sudden application of torque command of 100% is shown in Fig. 14. It is seen that the torque response of the proposed DTC based on a 12-sided polygonal space vector scheme is faster than the conventional DTC based on the hexagonal space vector scheme.

Here, the torque command is given at time when the stator flux vector is along the α-axis. The voltage space vector $\vec{V}_3$ or $\vec{V}_4$ can be applied for DTC based on a 12-sided space vector, and $\vec{V}_2$ or $\vec{V}_3$ can be applied for DTC based on a hexagonal space vector. If any of these voltage space vectors are applied for a time Δt, then the *q*-axis component of the applied voltage space vector is given as

$$V_{sq,6} = V_{\rm DC}\sin(60^{\rm o}) = 0.866\ V_{\rm DC} \tag{24}$$

$$V_{sq,12} = V_{\rm DC}\sin(75^{\rm o}) = 0.966\ V_{\rm DC}. \tag{25}$$

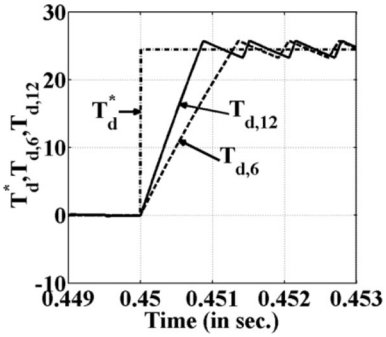

Fig. 14. Torque response of DTC based on a 12-sided polygonal space vector and DTC based on a hexagonal space vector for step change in reference torque to 100% of rated torque.

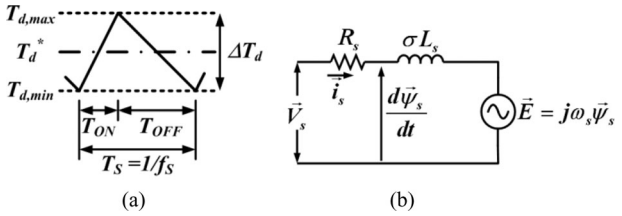

Fig. 15. (a) Torque variation for one switching cycle in hysteresis band for constant stator flux. (b) Equivalent circuit of an induction motor with back emf.

The q-axis component of the applied voltage space vector for a 12-sided space vector is higher than the applied space vector for the hexagonal structure, as from (24) and (25). This higher value of the q-axis component will result in a higher value of angle $(\rho_s - \rho_r)$. This higher value of angle $(\rho_s - \rho_r)$ will result in fast torque development which is seen in Fig. 14.

B. Comparison of Switching Frequency Variation in a Sector

The switching frequency variation of the proposed DTC based on a 12-sided polygonal space vector is compared with the conventional DTC based on the hexagonal space vector, for the whole range of speed of operation. The switching frequency at a given position of the stator flux is derived using the torque error equation where the stator flux is assumed constant for one switching cycle. The one switching cycle consists of switching of an active vector followed by a zero vector. The derivation of switching frequency is given later.

The torque equation of the induction motor is given by

$$T_d = \frac{2}{3}\frac{P}{2}\left(\vec{\psi}_s \times \vec{i}_s\right). \tag{26}$$

If the stator flux is assumed constant, then the change in torque during one switching cycle is given by ΔT_d as shown in Fig. 15(a). Hence, the change in torque is given by

$$\Delta T_d = \frac{2}{3}\frac{P}{2}\left(\vec{\psi}_s \times \Delta\vec{i}_s\right). \tag{27}$$

The change in torque can be calculated using the calculated value of$\Delta\vec{i}_s$. The value of $\Delta\vec{i}_s$ will be calculated using the

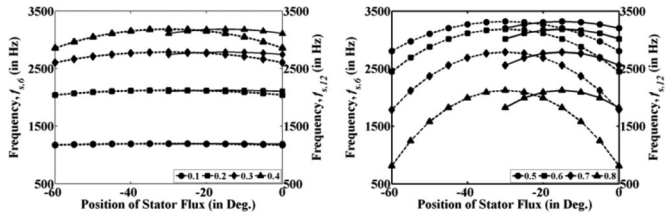

Fig. 16. Switching frequency variation of 12-sided DTC and 6-sided DTC. (a) For back emf variation from 0.1 to 0.4. (b) For back emf variation from 0.5 to 0.8.

equivalent circuit with $R_s\vec{i}_s$ drop neglected [see Fig. 15(b)] as

$$\Delta\vec{i}_s = \frac{\vec{V}_s - \vec{E}}{\sigma L_s}\Delta t. \tag{28}$$

The value of $\Delta\vec{i}_s$ from (28) is put into (27) to yield Δt as

$$\Delta t = \frac{3}{2}\frac{2}{P}\frac{\Delta T_d \sigma L_s}{(\vec{\psi}_s \times (\vec{V}_s - \vec{E}))}. \tag{29}$$

Equation (29) gives the time duration of the switching vector for the known value of torque ripple ΔT_d, stator flux vector $\vec{\psi}_s$, inverter output vector $\vec{V}_s$, and modulation index of operation (or frequency of operation).

The time duration $T_{\rm ON}$ and $T_{\rm OFF}$ is calculated for the application of the active vector and zero vector, respectively.

The time duration of switching of the active vector is

$$T_{\rm ON} = \frac{3}{2}\frac{2}{P}\frac{\Delta T_d \sigma L_s}{(\vec{\psi}_s \times (\vec{V}_s - \vec{E}))}. \tag{30}$$

The time duration of switching of the zero vector is

$$T_{\rm OFF} = \frac{3}{2}\frac{2}{P}\frac{\Delta T_d \sigma L_s}{(\vec{\psi}_s \times -\vec{E})}. \tag{31}$$

The time period T_S of one switching cycle is

$$T_S = \frac{1}{f_S} = T_{\rm ON} + T_{\rm OFF}. \tag{32}$$

Hence, the switching frequency f_S is calculated using (32).

The switching frequency f_S variation is plotted in Fig. 16 for both DTC schemes. The plot with a solid line is for a 12-sided space vector and the plot with a dashed line is for a hexagonal space vector. The switching frequency f_S is calculated for a stator flux position varying from -60° to 0° for a hexagonal space vector and from -30° to 0° for a 12-sided polygonal space vector.

The stator flux position is varied considering active vector switching duration of 60° in a hexagonal space vector-based PWM control and 30° in a 12-sided polygonal space vector-based PWM control. The switching frequency variation is plotted for different values of modulation index (i.e., variation of $\vec{E}$) which varied from 0.1. to 0.8 p.u. for torque ripple ΔT_d of 10% of rated value, stator flux vector $\vec{\psi}_s$ of rated value, inverter output vector $\vec{V}_s$ of vector length of 500 V. Fig. 16(a) and (b) shows the switching frequency variation for a modulation

index which varied from 0.1 to 0.4 p.u. and from 0.5 to 0.8 p.u, respectively.

It can be seen in Fig. 16 that the frequency variations for the DTC scheme based on 12-sided polygonal space vectors are less compared to a conventional DTC scheme based on hexagonal space vectors. The frequency variation is the same for a lower modulation index of operation as shown in Fig. 16(a). But the frequency variation is increasing as modulation index is increasing. The frequency variation is more for a hexagonal space vector-based DTC scheme for higher modulation as shown in Fig. 16(b).

VI. Conclusion

A variable speed DTC scheme for an open-end induction motor drive based on a 12-sided polygonal space vector using the fundamental stator voltage for sector identification is proposed for the first time. The novelty of the proposed scheme lies in the application of the estimated fundamental stator voltage vector, in selecting the sector and then the inverter switching vectors, for the DTC control using the 12-sided polygonal voltage vectors. This also improves the accuracy of the voltage vector selection, for the entire speed range, resulting in higher dynamics of torque control. The proposed estimation method of the fundamental stator voltage is very simple and uses the steady-state model of the induction motor. Therefore, the proposed DTC scheme utilizes the exact positions of the fundamental stator voltage vector and stator flux vector to select an optimal switching vector for fast control of torque, with small variation of stator flux within the hysteresis band. The switching voltage vector selection based on sector information of the fundamental stator voltage vector and the relative position of the stator flux permit the DTC drive to operate at a very low speed of around 1 Hz, with fast control of the full rated torque. The proposed drive can be effectively operated for zero speed with full load applied (i.e., the DTC drive can be operated at zero speed). Standard stator resistance parameter adaptation techniques are available in the literature and it can be easily incorporated in to this study as well. The proposed DTC scheme has been implemented for experimental verification using a DSP processor. Extensive experimental results are shown at various speeds of operation up to 1 Hz to verify the proposed concept. The same control scheme is further extended from 1 to rated 50 Hz operation of the inverter. Among the advantages achieved by the proposed 12-sided polygonal space vector-based DTC are fast torque transient, increased modulation range, reduced switching frequency variation, and possible operation up to zero speed. The experimental results prove that the proposed fundamental stator voltage-based DTC scheme for an induction motor drive can be utilized for an electrical vehicle application.

Appendix

IM parameters: 3.7 kW, 3Φ, four poles, 415 V, 50 Hz, 1445 r/min, $R_s = 4.8\ \Omega$, $R_r = 3.8\ \Omega$, $L_s = 0.5632$ H, $L_r = 0.577$ H, $M = 0.546$ H, moment of inertia, $J = 0.1\ \text{kg}\cdot\text{m}^2$.

Acknowledgment

The authors would like to thank CiSTUP, the Indian Institute of Science, Bangalore, for providing the funds to build the experimental setup at the Center for Electronics Design and Technology, Indian Institute of Science, Bangalore.

References

[1] G. S. Buja and M. P. Kazmierkowski, "Direct torque control of PWM inverter-fed AC motors—A survey," *IEEE Trans. Ind. Electron.*, vol. 51, no. 4, pp. 744–757, Aug. 2004.

[2] D. Casadei, F. Profumo, G. Serra, and A. Tani, "FOC and DTC: Two viable schemes for induction motors torque control," *IEEE Trans. Power Electron.*, vol. 17, no. 5, pp. 779–787, Sep. 2002.

[3] I. Takahashi and T. Noguchi, "A new quick-response and high-efficiency control strategy of an induction motor," *IEEE Trans. Ind. Appl.*, vol. IA-22, no. 5, pp. 820–827, Sep. 1986.

[4] M. Depenbrock, "Direct self-control (DSC) of inverter-fed induction machine," *IEEE Trans. Power Electron.*, vol. 3, no. 4, pp. 420–429, Oct. 1988.

[5] J. H. Ryu, K. W. Lee, and J. S. Lee, "A unified flux and torque control method for DTC-based induction-motor drives," *IEEE Trans. Power Electron.*, vol. 21, no. 1, pp. 234–242, Jan. 2006.

[6] S. Kouro, R. Bernal, H. Miranda, C. A. Silva, and J. Rodriguez, "High-performance torque and flux control for multilevel inverter fed induction motors," *IEEE Trans. Power Electron.*, vol. 22, no. 6, pp. 2116–2123, Nov. 2007.

[7] K.-K. Shyu, J.-K. Lin, V.-T. Pham, M.-J. Yang, and T.-W. Wang, "Global minimum torque ripple design for direct torque control of induction motor drives," *IEEE Trans. Ind. Electron.*, vol. 57, no. 9, pp. 3148–3156, Sep. 2010.

[8] Y. S. Lai and J. H. Chen, "A new approach to direct torque control of induction motor drives for constant inverter switching frequency and torque ripple reduction," *IEEE Trans. Energy Convers.*, vol. 16, no. 3, pp. 220–227, Sep. 2001.

[9] C. Lascu and A. M. Trzynadlowski, "A sensorless hybrid DTC drive for high-volume low-cost applications," *IEEE Trans. Ind. Electron.*, vol. 51, no. 5, pp. 1048–1055, Oct. 2004.

[10] C. Lascu, I. Boldea, and F. Blaabjerg, "Variable-structure direct torque control—A class of fast and robust controllers for induction machine drives," *IEEE Trans. Ind. Electron.*, vol. 51, no. 4, pp. 785–792, Aug. 2004.

[11] Y. Zhang, J. Zhu, Z. Zhao, W. Xu, and D. G. Dorrell, "An improved direct torque control for three-level inverter-fed induction motor sensorless drive," *IEEE Trans. Power Electron.*, vol. 99, Feb. 2010.

[12] T. Geyer, G. Papafotiou, and M. Morari, "Model predictive direct torque control. Part I: Concept, algorithm, and analysis," *IEEE Trans. Ind. Electron.*, vol. 56, no. 6, pp. 1894–1905, Jun. 2009.

[13] T. Geyer, "Computationally efficient model predictive direct torque control," *IEEE Trans. Power Electron.*, vol. 26, no. 10, pp. 2804–2816, 2011.

[14] R. Vargas, U. Ammann, B. Hudoffsky, J. Rodriguez, and P. Wheeler, "Predictive torque control of an induction machine fed by a matrix converter with reactive input power control," *IEEE Trans. Power Electron.*, vol. 25, no. 6, pp. 1426–1438, Jun. 2010.

[15] T. Noguchi, M. Yamamoto, S. Kondo, and I. Takahashi, "Enlarging switching frequency in direct torque-controlled inverter by means of dithering," *IEEE Trans. Ind. Appl.*, vol. 35, no. 6, pp. 1358–1366, Dec. 1999.

[16] C. Lascu, I. Boldea, and F. Blaabjerg, "Direct torque control of sensorless induction motor drives: A sliding-mode approach," *IEEE Trans. Ind. Appl.*, vol. 40, no. 2, pp. 582–590, Apr. 2004.

[17] S. Mir and M. E. Elbuluk, "Precision torque control in inverter-fed induction machines using fuzzy logic," in *Proc. 26th Annu. IEEE Power Electron. Spec. Conf.*, Atlanta, GA, vol. 1, Jun. 18, 1995, pp. 396–401.

[18] T. G. Habetler, F. Profumo, M. Pastorelli, and L. M. Tolbert, "Direct torque control of induction machines using space vector modulation," *IEEE Trans. Ind. Appl.*, vol. 28, no. 5, pp. 1045–1053, Oct. 1992.

[19] M. P. Kazmierkowski and A. B. Kasprowicz, "Improved direct torque and flux vector control of PWM inverter-fed induction motor drives," *IEEE Trans. Ind. Electron.*, vol. 42, no. 4, pp. 344–350, Aug. 1995.

[20] C. Lascu, I. Boldea, and F. Blaabjerg, "Direct torque control of sensorless induction motor drives: A sliding-mode approach," *IEEE Trans. Ind. Appl.*, vol. 40, no. 2, pp. 582–590, Apr. 2004.

[21] G. Buja, D. Casadei, and G. Serra, "Direct stator flux and torque control of an induction motor: theoretical analysis and experimental results," in *Proc. 24th Annu. Conf. IEEE Ind. Electron. Soc.*, Aachen, Germany, Sep. 31, 1998, vol. 1, pp. T50–T64.
[22] K. K. Mohapatra, K. Gopakumar, V. T. Ranganathan, and L. Umanand, "A harmonic elimination and suppression scheme for an open-end winding induction motor drive," *IEEE Trans. Ind. Electron.*, vol. 50, no. 6, pp. 1187–1198, Dec. 2003.
[23] J. Quan and J. Holtz, "Sensorless vector control of induction motors at very low speed using a nonlinear inverter model and parameter identification," *IEEE Trans. Ind. Appl.*, vol. 38, no. 4, pp. 1087–1095, Aug. 2002.
[24] S. Bhattacharya, A. Veltman, D. M. Divan, and R. D. Lorenz, "Flux-based active filter controller," *IEEE Trans. Ind. Appl.*, vol. 32, no. 3, pp. 491–502, Oct. 1996.
[25] T. Bhattacharya and L. Umanand, "Improved flux estimation and stator-resistance adaptation scheme for sensorless control of induction motor," *IEE Proc.—Electr. Power Appl.*, vol. 153, no. 6, pp. 911–920, Nov. 2006.
[26] C. Patel, R. Ramchand, K. Sivakumar, A. Das, and K. Gopakumar, "A rotor flux estimation during zero and active vector periods using current error space vector from a hysteresis controller for a sensorless vector control of IM drive," *IEEE Trans. Ind. Electron.*, vol. 58, no. 6, pp. 2334–2344, Jun. 2011.
[27] A. S. Bharadwaj and R. Krishnan, "A review of parameter sensitivity and adaptation in indirect vector controlled induction motor drive systems," *IEEE Trans. Power Electron.*, vol. 6, no. 4, pp. 695–703, Oct. 1991.
[28] T. G. Habetler, F. Profumo, G. Griva, M. Pastorelli, and A. Bettini, "Stator resistance tuning in a stator-flux field-oriented drive using an instantaneous hybrid flux estimator," *IEEE Trans. Power Electron.*, vol. 13, no. 1, pp. 125–133, Jan. 1998.
[29] V. Ebenezer, K. Gopakumar, and V. T. Ranganathan, "A sensorless vector control scheme for induction motor using a space phasor based current hysteresis controller," *EPE J.*, vol. 9, no. 3–4, pp. 41–46, Jan. 2000.

Chintan Patel (S'08) received the B.E. degree in electrical engineering from South Gujarat University, Surat, India, in 2000, the M.Tech. degree from Institute of Technology, Banaras Hindu University, Varanasi, India, in 2003, and the Ph.D. degree from Center for Electronics Design and Technology, Indian Institute of Science, Bangalore, India, in 2011.

He is currently a Research Fellow at The University of Nottingham, Nottingham, U.K. His research interests include sensorless vector control and DTC of induction motors and hysteresis current controller.

Rajeevan P. P. received the B.Tech. degree in electrical engineering from the University of Calicut, Kerala, India, and the M.E degree in power electronics from Bangalore University, Bangalore, India. He is currently working toward the Ph.D degree at Centre for Electronics Design and Technology, Indian Institute of Science, Bangalore, India.

His research interests include multilevel power converters, drives, PWM techniques, and power quality.

Anubrata Dey received the B.E. degree in electrical engineering from Jalpaiguri Government Engineering College, Jalpaiguri, India, in 2002, and the M.Tech. degree in control system from Bengal Engineering and Science University, Kolkata, India, in 2005. He is currently working toward the Ph.D. degree at the Center for Electronics Design and Technology, Indian Institute of Science, Bangalore, India.

From 2006 to 2008, he was with the Indian Space Research Organisation, Bangalore, India, and from 2008 to 2009, he was with the GE India Technology Centre Pvt. Ltd., Bangalore, India. His research interests include multilevel inverter fed drives and control.

Rijil Ramchand (S'09) received the B.Tech. degree in electrical engineering from Calicut University, Thenhipalam, India, in 1996, and the M.E. degree from Indian Institute of Science in 2008, and the Ph.D. degree from the Centre for Electronics Design and Technology, Indian Institute of Science, Bangalore, India, in 2010.

He is a Faculty Member with the Department of Electrical Engineering, National Institute of Technology, Calicut, India. His research interests include power converters, pulse width modulation techniques, and ac drives.

K. Gopakumar (M'94–SM'96) received the B.E., M.Sc. (Engg.), and Ph.D. degrees from the Indian Institute of Science, Bangalore, India, in 1980, 1984, and 1994, respectively.

He was with the Indian Space Research Organization, Bangalore, India, from 1984 to 1987. He is currently a Chairman and Professor at the Center for Electronics Design and Technology, Indian Institute of Science. His research interests include PWM converters and high power drives.

Dr. Gopakumar is a Fellow of Institution of Electrical and Telecommunication Engineers, India and Indian National Academy of Engineers. He is currently an Associate Editor of IEEE Transaction on Industrial Electronics.

Marian P. Kazmierkowski (M'89–SM'91–F'98) received the M.S., Ph.D., and Dr. Sci. degrees in electrical engineering from the Institute of Control and Industrial Electronics (ICIE), Warsaw University of Technology, Poland, in 1968, 1972, and 1981, respectively.

From 1987 to 2008, he was the Director of ICIE. Since 2003 he has also been the Head of the Centre of Excellence on Power Electronics Intelligent Control for Energy Conservation (PELINCEC) at ICIE. He is currently the Dean of the Department of Technical Science, Polish Academy of Science, Warsaw, Poland.

Dr. Kazmierkowski was the recipient of an Honorary Doctorate degree from Aalborg University in 2004 and from the Institut National Polytechnique de Toulouse, France, in 2010. In 2005 he received the Dr.-Ing. Eugene Mittelmann Achievement Award from the IEEE Industrial Electronics Society and in 2007 the SIEMENS Research Award in Poland. In 2007, he was a Corresponding Member of the Polish Academy of Science. He was the Editor-in-Chief of the IEEE TRANSACTIONS ON INDUSTRIAL ELECTRONICS from 2004 to 2006.